Chalcogenide Letters Vol. 18, No. 6, June 2021, p. 339 - 349

Octadecyl amine capped cadmium sulfide quantum dots: morphological studies, electrochemical properties, and its use as photocatalyst for the degradation of methylene blue dyes

P. A. Ajibade*, N. K. Mkhwanazi, L. L.R. Mphahlele
School of Chemistry and Physics, University of KwaZulu-Natal, Private Bag X01, Scottsville, Pietermaritzburg 3209, South Africa

We present the structural, optical, electrochemical, and photocatalytic studies of octadecyl amine capped CdS quantum dots (ODA-CdS). TEM micrographs showed CdS quantum dots with particle sizes of 1.9-5.2 nm. The optical bandgaps of the quantum dots are 2.03, 2.06 and 2.01 eV for ODA-CdS**1**, ODA-CdS**2** and ODA-CdS**3** respectively, which was less than the bandgap of the bulk CdS (2.42 eV). Photo-electrochemical band gaps of 2.60 V for ODA-CdS**1**, 2.24 V for ODA-CdS**2** and 2.46 V for ODA-CdS**3** were obtained from cyclic voltammetry. The photocatalytic degradation efficiency of methylene blue was 62% for ODA-CdS**1**, 80% for ODA-CdS**2**, 69% for ODA-CdS**3**.

(Received March 23, 2021; Accepted June 24, 20121)

Keywords: Cadmium sulfide, Quantum dots, Single-source precursor, Structural studies, Photocatalytic degradation, Methylene blue

1. Introduction

The problem of environmental pollution from industrial waste affects both developing and developed countries [1]. Most textile dyes waste emanate from processing plants and cause contamination and eutrophication in water bodies biological system [2] [3]. In recent years, more environmental standards and regulations have led to the development of several strategies to remove dyes waste [4, 5]. These include chemical (chlorination, ozonation), physical (adsorption) and biological (biodegradation) techniques [6-8]. The use of photocatalysis as decontamination techniques in wastewater treatment has shown excellent results for most dyes [9-11]. The use of nanocrystals as photocatalysts to remove pollutants such as dyes are being explored [12, 13]. There are two distinct types of photocatalysts for water treatment: Sun oriented photocatalyst and photocatalytic instruments equipped with ultraviolet (UV) light [14, 15]. Most group II-IV compound semiconductors such as CdS, CdSe, ZnS, ZnO are studied under UV irradiation with high-pressure lamps at different wavelengths. CdS semiconductors are the most studied among II-IV compound semiconductors due to its bandgap (2.42 eV) and size-dependent properties in relation to their corresponding bulk material [16-18]. The band theory suggests that the valence and conduction band divide the bandgap with energetic range for semiconductors between 0.7-3.5 eV [19, 20]. Most quantum dots have electronic properties which include electrical conductivity which depend on the bandgap size [21]. For quantum dots to absorb light, the energy of the light source must be equal or greater than the bandgap energy (Eg) [22]. Such light absorption is used for photo degradation of organic pollutants such as dyes [23]. In this study, we report the structural, optical, and electrochemistry of CdS quantum dots prepared from three dithiocarbamate single-source precursors. The as-prepared CdS were used as photocatalysts for the degradation of methylene blue (MB) dye. The optical band gaps and the electrochemical band gaps of the quantum dots were compared.

* Corresponding author: ajibadep@ukzn.ac.za

https://doi.org/10.15251/CL.2021.186.339

2. Experimental

2.1. Chemicals and solvents

All reagents were purchased from Merck and used as obtained without further purification. Phenylpiperazine, imidazole, n-hexylanaline, cadmium nitrate tetrahydrate, tetrabutylammonium hexafluorophosphate, octadecylamine (ODA), oleic acid, methanol, ethanol, acetone, chloroform, dichloromethane, tetrahydrofuran, dimethyl sulfoxide, diethyl ether, sodium hydroxide, acetonitrile. The ligands were prepared following literature procedures: Sodium salt of phenylpiperazine dithiocarbamate ligand (L^1) [24, 25], sodium salt of imidazole dithiocarbamate ligand (L^2) [26], sodium salt of n-hexylaniline dithiocarbamate ligand (L^3) [27].

2.2. Synthesis of cadmium(II) complexes

2.2.1. Synthesis of cadmium(II) phenylpiperazine dithiocarbamate complex (C1).

Aqueous solution of cadmium nitrate tetrahydrate (3.085 g, 0.01 mol) in 20 mL of water was added with constant stirring to an aqueous solution of (5.210 g, 0.02 mol) of sodium salt 1-phenylpiperazine dithiocarbamate ligand dissolved in water. The resulting mixture was stirred at room temperature for 5 h. The product was filtered and washed with water and then with diethyl ether and dried under vacuum [24]. Yield: 0.211 g (48 %), Fourier-transform infrared FTIR (cm^{-1}): 1505 (νC-N), 999 (νC-S).

2.2.2. Synthesis of cadmium(II) imidazolyl dithiocarbamate complex (C2).

Imidazole dithiocarbamate ligand (3.324 g, 0.02 mol) was dissolved in 10 mL of distilled water. Cadmium nitrate (2.3642 g, 0.01 mol) was dissolved in an equivalent amount of water. The two solutions were mixed and stirred immediately. The reaction occurred at room temperature for 5 h. The resulting product was filtered, washed with deionized water followed by diethyl ether and dried [25]. Yield: 3.325 g (83 %), FTIR (cm^{-1}): 1470 (νC-N), 993 (νC-S).

2.2.3. Synthesis of cadmium(II) n-hexylaniline dithiocarbamate complex (C3)

Cadmium(II) n-hexylaniline dithiocarbamate complex was prepared by adding an aqueous solution of sodium salt of n-hexylaniline dithiocarbamate (0.0583 g, 0.0002 mol) to an aqueous solution of $Cd(NO_3)_2{\cdot}4H_2O$ (0.0308 g, 0.001 mol), the resulting mixture was stirred for 5 h. The precipitate formed was filtered, washed several times with distilled water and dried under vacuum [26]. Yield: 0.021 g (37 %), FTIR (KBr, cm^{-1}): 1410 (νC-N), 958 (νC-S). ^{1}H NMR (400 MHZ, D_2O-d^6): δ (ppm) = CH- protons -0.811 (t, 6H), CH- protons -1.227-1.249 (M, 12H), C-H-protons-1.634 (3, 4H), C-H- proton- 4.267 (t, 4H), C-H- proton- 7.437-7.446 (t, 4H), C-H- proton- 7.351-7.377 (t, 4H), C-H- proton- 7.2126 (t, 2 H). 13C NMR (400 MHz, D_2O-d6) δ (ppm): Ca- 1174.27 (C-H), Cb- 173.50 (C-H), Cc- 109.51 (C-H), Cd- 77.51 (C-H), Ce- 72.31 (C-H), Cf- 72.31-73.30 (C-H), Cg- 60.53 (C-H), Ch- 192.92 (C-N), Ci- 175.63 (C-C).2.3.

2.3. Synthesis of CdS quantum dots from Cd(II) dithiocarbamate single source precursors

Cadmium sulfide quantum dots were thermolysed at three different temperatures, (C1) at 120 ℃, (C2) at 180 ℃, and (C3) at 220 ℃. 250 mg of each complex was dispersed in 6 mL of oleic acid, the mixture was then added to 3.00 g of hot octadecylamine (ODA). The system was plugged with nitrogen stirred at 400rp for an hour. The product was cooled to 70 °C, and methanol was added to remove extra capping agent. The resulting precipitate was separated by centrifugation at 2000 rpm for 30 mins [27].

2.4. Physical measurements

FTIR spectra were recorded on a Carry 630 FTIR spectrometer. Bruker ultra-shield 400 NMR spectrometer using 400.1 MHz for ^{1}H and 100.6 MHz for ^{13}C nuclei for proton and carbon confirmation. Mass spectra were obtained from Shimadzu LCMS-2020. Ultraviolet-visible (UV-Vis) spectra and photocatalysis of the compounds were confirmed from Perkin Elmer Lambda 35 UV-Vis spectrometer. Powder X-ray diffraction (pXRD) was obtained on Philips PW1830 X-ray diffractometer. Transmission electron microscope (TEM) micrographs were obtained using the

Joel 1400 TEM and the high-resolution transmission electron microscope (HRTEM) micrographs were obtained using the JEOL HRTEM 2100. Scanning electron microscope (SEM) and energy dispersive spectroscopy (EDS) images were obtained from ZEISS EVO LS 15 SEM. Perkin Elmer LS 45 fluorescence spectrometer was used for photoluminescence studies while Potentiostat/Galvanostat was used for electrochemistry.

2.5. Optical and Electrochemical analysis of CdS quantum dots

The optical band gap was obtained from a mixture of 5 mg of nanocrystals in 20 mL of chloroform and was analysed using a UV-Vis spectrophotometer at room temperature. The cyclic voltammetry was carried out at room temperature under nitrogen using Auto-Lab Potentiostat/Galvanostat (with Nova 1.3 software) with 3 electrodes. Ag wire and Pt wire were used as working, quasi-reference, and counter electrodes. 2 mM solution of the CdS and 0.1 M tetrabutylammonium hexafluorophosphate (TBAPF6) supporting electrolyte was prepared in N,N-Dimethylformamide (DMF) [28, 29].

2.6. Photocatalytic study of methylene blue dye

Photocatalytic degradation of methylene blue by the CdS quantum dots on was carried out using OSRAM VIALOX (65600 lumens) high-pressure sodium lamp. The quantum dots nano-photocatalyst was first dispersed in an aliquot of methylene blue solution. The solution with the catalyst was sonicated for 20 min and further stirred in the dark for 15 min for the solution to be well dispersed so that the loss of compound due to adsorption can be measured. The mixture was illuminated for three hours and the photodegradation of the dye was studied by a UV-Vis spectrophotometer at 660 nm [30, 31].

3. Results and discussion

3.1. Spectroscopic studies of both dithiocarbamate ligands and complexes

Upon careful analysis, the infrared spectra of the ligands and cadmium complexes are compared. The stretching frequency at 1428 cm^{-1} for C1, 1442 cm^{-1} for C2, and 1550 cm^{-1} for C3 are assigned to the ν(C–N) stretching mode in the ligands FTIR spectra, which shifted in the spectra of the complexes to 1505 cm^{-1} for C1, 1470 cm^{-1} for C2, and 1410 cm^{-1} for C3. This suggests a single bond order for the C-N attributed to the formation of cadmium(II) complexes and the delocalization of the dithiocarbamate electrons from the ligands. The N-CSS mode shifted to higher wave number upon coordination, indicating an increase in the double bond character of the carbon-nitrogen bond due to electron delocalization to the cadmium core. Two peaks within the range of 998-1214 cm^{-1} for L^1, 973-1150 cm^{-1} for L^2, and 950-1100 cm^{-1} for L^3 are assigned respectively to the symmetric and asymmetric vibrations of ν(C-S). The complexes had sharp single bands at 999 cm^{-1} for C1, 993 cm^{-1} for C2, and 958 cm^{-1} for C3 [32].

^{1}H and ^{13}C NMR spectra for 1-phenylpiperazine, imidazole, and n-hexylanaline dithiocarbamate ligand displayed all the expected signals and the chemical shifts. These peaks confirm the formation of the ligand. These results are comparable with the literature results [33]. The corresponding complexes had poor solubility in almost all the solvent, which made it impossible to perform any solution based analysis [34]. All the mass spectra for dithiocarbamate ligands show parent peaks as well as peaks due to molecular ions and the molecular mass of these ligands.

3.2. Powder X-ray diffraction studies of the CdS quantum dots

Powder XRD diffraction patterns of the octadecylamine capped cadmium sulfide (ODA-CdS) quantum dots (Fig. 1) exhibited well-diffracted peaks at 20°, 25°, 30°, 45°, and 55° corresponding to (100), (111), (200), (220), and (311) indices of zinc blende crystal structure of CdS (JCPDS 75-0581) [35]. All the CdS quantum dots have the same diffraction patterns irrespective of the precursor used which could be attributed to using the same capping agent for the preparation. The XRD patterns indicate the as-synthesized CdS quantum dots are almost in pure cubic zinc blende phase with small traces of hexagonal phase indexed to (#216) structure with

space group F43m for all the CdS quantum dots [36]. The sharp peaks observed the PXRD diffractograms confirm the CdS quantum dots have small crystallite sizes.

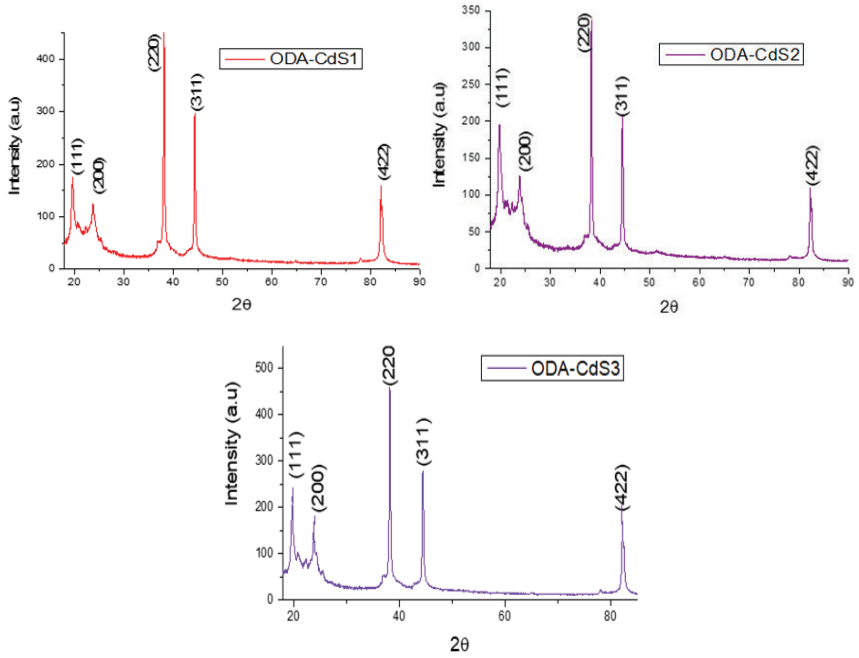

Fig. 1. XRD patterns of the cadmium sulphide quantum dots.

3.3. Microscopy studies of the octadecyl amine capped CdS quantum dots

TEM micrograph of the ODA-CdS quantum dots is presented in Figure 2. The TEM micrograph of ODA-CdS**1** quantum dots (Figure 2a) prepared at 120 ℃ from cadmium complex of phenylpiperazine, revealed sphere-shaped monodispersed quantum dots with crystallite size of 1.9-2.0 nm. The micrograph of the lattice fringes (Figure 2b) showed uniform particles distribution with a standard deviation of 1.40 nm (histogram fitting Figure 3a) and interplanar distances of 0.30 and 0.32 nm. The selected area diffraction (SAED) patterns (Figure 2c) showed that quantum dots are crystalline in nature due to bright spots that form rings patterns. TEM micrograph of ODA-CdS**2** quantum dots (Figure 2e) prepared from imidazole cadmium(II) complex showed spherically shaped particles with some agglomeration with the crystallite size in the range 2.3-4.7 nm. The histogram fitting (Figure 3b) gives mean 0.58 nm with standard deviation of 0.37 nm which is high compared to the mean due to the wide distribution of the particles. The lattice fringes (Fig 2e) showed nanopolycrystalline particles with a d-spacing of 0.32 nm. Figure 2(e) shows SAED of ODA-CdS2 which displayed blurring contrast due to some amorphous layer ascribed to deposition of capping agent that diminishes the lattice fringes contrast.

TEM micrograph of ODA-CdS3 (Fig. 2g) showed sphere-shaped particles with crystallite size of 3.22-5.21 nm. Figure 2h shows lattice fringes with random distribution of 1.34 nm crystalline particles with d-spacing of 2.1 nm, the distribution is evidenced by the histogram fitting (Fig. 3c) with the standard deviation of 1.3 nm. SAED of the ODA-CdS**3** quantum dots (Fig. 2i) displayed a well-differentiated diffraction pattern with tiny bright spots forming rings attributed to the single quantum dots.

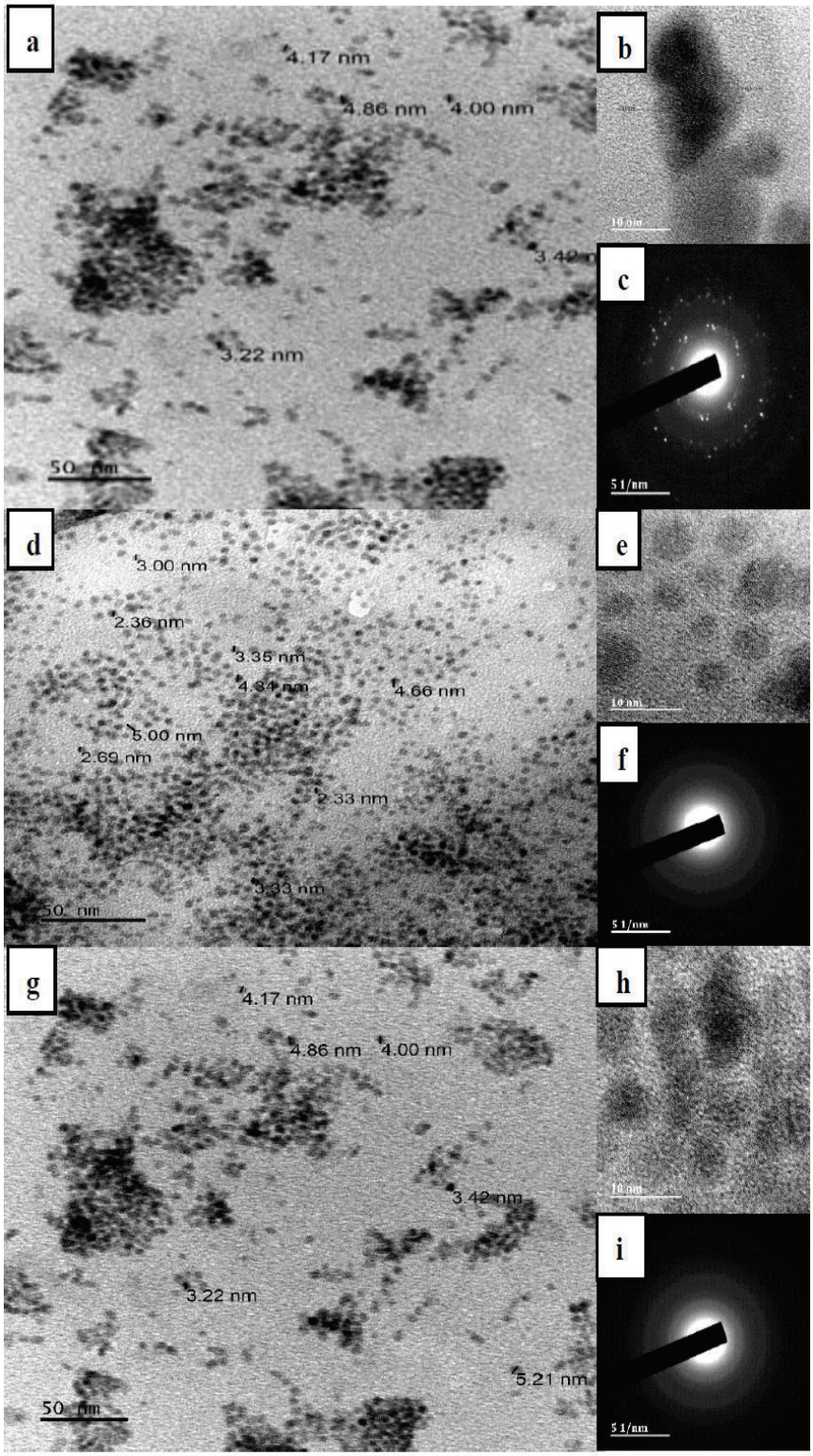

Fig. 2. TEM micrographs (a, d, and g), lattice fringes (b, e, and g) and SAED (c, f, and i) of ODA-CdS1, ODA-CdS2 and ODA-CdS3 quantum dots respectfully.

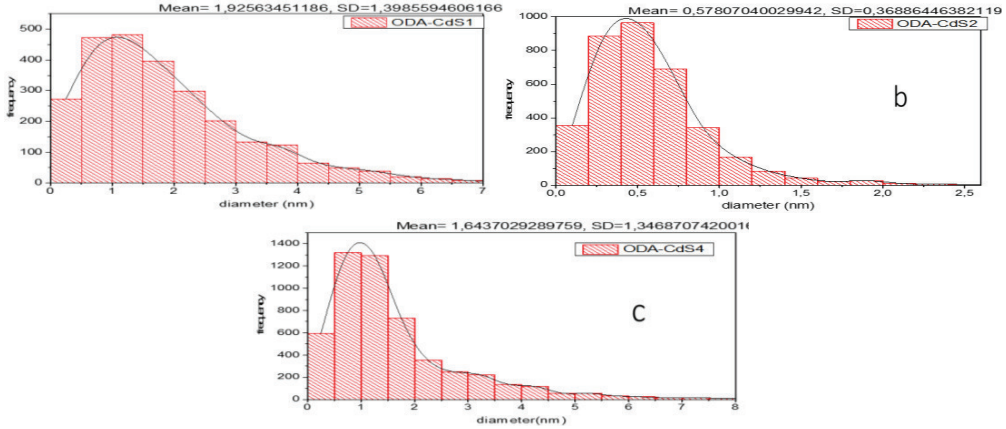

*Fig. 3. Size distribution of ODA-CdS1 (a), ODA-CdS2 (b), and ODA-CdS**3** (c) as-prepared quantum dots.*

SEM studied the surface morphology of ODA-CdS quantum dots. The SEM images of ODA-CdS**1** (Fig. 4a) showed a lumpy particle with holes on the surface.

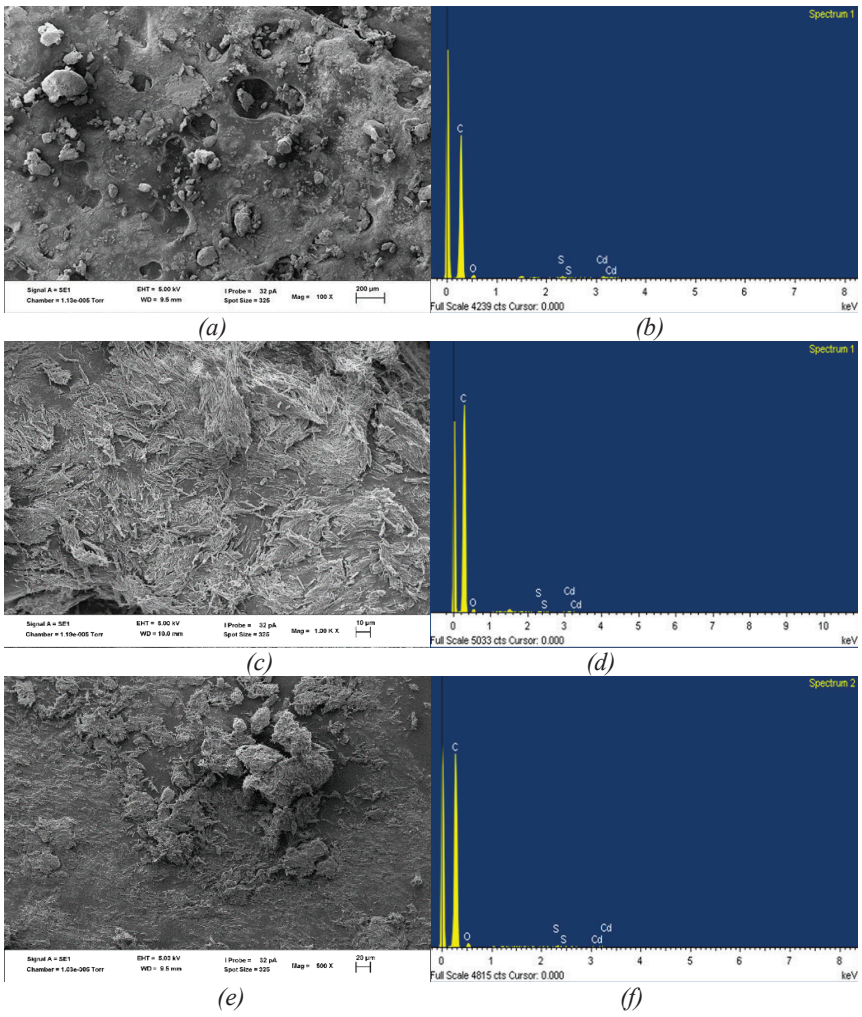

Fig. 4. SEM micrograph (a, c, and e) and EDS (b, d, and f) spectra of ODA-CdS quantum dots.

SEM image of ODA-CdS**2** (Fig. 4c) shows flaky strew like surface with some lumps and thin particles with no form or pattern, but it has a uniform distribution. Fig. 4e shows surface morphology of ODA-CdS**3**, as wool-like surface morphology with large and small particles sparsely distributed on the surface. Elemental composition of the nanoparticles obtained from the EDS as shown in Fig. 4 (b, d, e), shows the presence of C, O, S. Which confirms the preparation of CdS quantum dot and the C atom that is attributed to the carbon tape used upon analysis.

3.4. Optical studies of cadmium sulfide quantum dots

The absorption, Tauc plot and emission spectra of the ODA-capped CdS quantum dots are presented in Figure 5. The absorption spectra (Figure 5(a)) showed very sharp peaks at 250 nm for ODA-CdS1, ODA-CdS2, and ODA-CdS3. The optical absorption revealed that the nanocrystallite are blue shifted compared to the bulk nanoparticles due to quantum size effect. The fundamental absorption, which matches the excitation of electrons from occupied band to unoccupied band regulates the optical band gap size. The Tauc plot (Figure 5(b)) showed the determined energy band gap values which are deduced from the absorption data of the nanocrystallite, as calculated using the Brus equation [37]. The known bandgap energy for bulk CdS is 2.41 eV [38], the bandgap energies of the as-prepared CdS quantum dots are 2.03 eV for ODA-CdS1, 2.06 eV for ODA-CdS2, and 2.01 eV for ODA-CdS3 respectively. The energy band gap of the CdS quantum dots is narrow compared to that of the bulk CdS which indicates that the particles are nanosized as reported previously [39]. The photoluminescence spectra recorded at different excitation wavelengths showed broad emission maxima. ODA-CdS1 excited at 700 nm showed emission maximum at 685 nm, ODA-CdS2 excited at 750 nm showed emission peak at 698 nm, and ODA-CdS3 excited at 750 nm showed emission maximum at 731 nm. Comparison of the emission maxima and the absorption band edges confirmed that the emission peaks were red shifted. The increase in emission maxima could be ascribed to both the size and increase surface area [40].

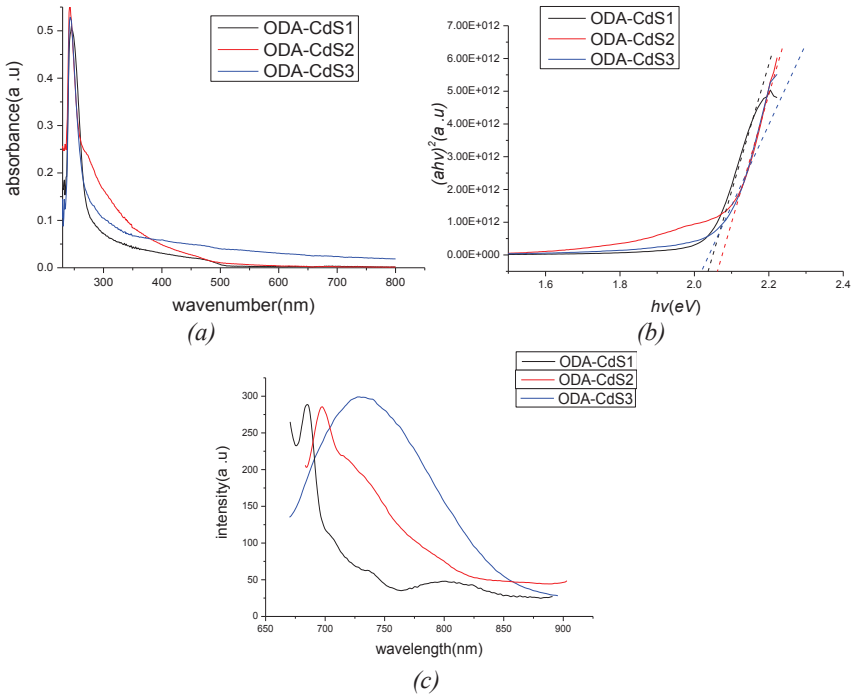

Fig. 5. The absorption spectra(a), tauc plot (b) and emission spectra (c)for ODA-CdS1, ODA-CdS2 and ODA-CdS3 excited at 700, 750 and 750 nm respectively.

3.5. Electrochemical band gap of the octadecylamine capped CdS quantum dots

Cyclic voltammetry (CV) can be used to measure the electrochemical bandgap, which is the energy gap between the oxidation and reduction peaks. The CV of the ODA capped CdS quantum dots showed similar features (Fig. 6 (a-c)). The oxidation signals were observed at approximately ~1-2.5 V while the reduction signal appeared at about ~-0.1 to – 2.5 V. From these results, the calculated electrochemical band gaps are 2.60 V for ODA-CdS**1**, 2.24 V for ODA-CdS**2**, and 2.46 V for ODA-CdS**3** respectively. The electrochemical band gaps are like the optical band gaps but slightly higher which indicates the quantum dots might be good for charge transfer applications. Varying the scan rate shows that ODA-CdS**1** and ODA-CdS**2** have similar oxidation-reduction characteristics with the reduction potential signal shifting towards the oxidation signal.

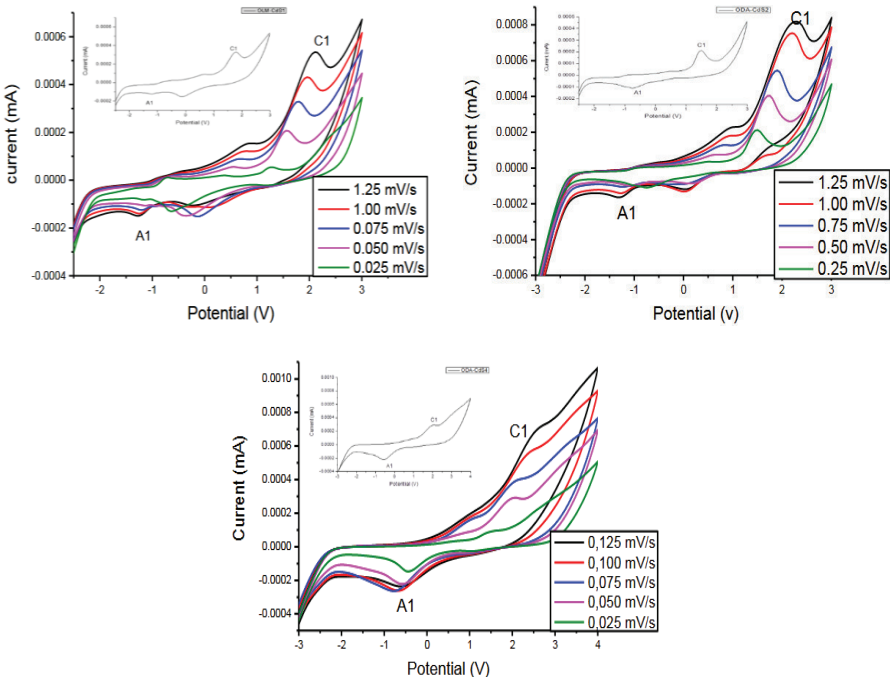

Fig. 6. Cyclic voltammogram of ODA-CdS quantum dots with five different scan rates.

3.6. Photocatalytic decomposition of methylene blue using different catalyst

The photocatalytic gradation of MB by the CdS quantum dots using OSRAM VIALOX (65600 lumens) high-pressure sodium lamp, which has regular light irradiation settings for evaluation of solar cell efficiency [34].

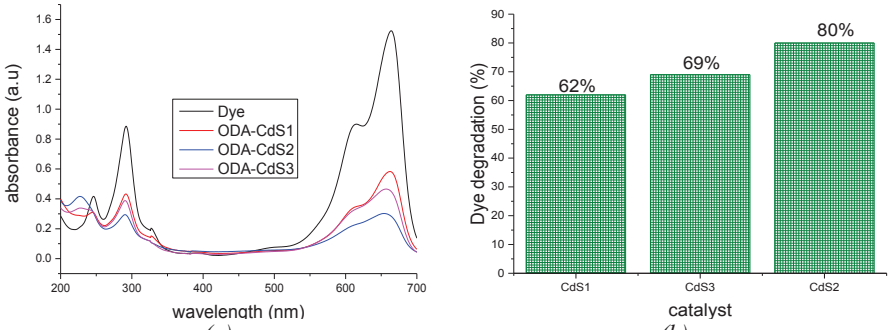

(a) *(b)*

Fig. 7. Absorption spectra of $[MB]_0$ = ppm degradation (a) and percentage degradation (b) of CdS quantum dots (ODA-CdS) under visible light irradiation.

During the degradation of organic dyes, parameter such as dye concentration affect the decomposition. The absorption spectra of MB after photocatalytic degradation by the CdS quantum dots are presented in Fig. 7(a). The percentage degradation of MB by the as-prepared quantum dots are 62% for ODA-CdS**1**, 80% for ODA-CdS**2**, and 69% ODA-CdS**3** (Fig. 7b). ODA-CdS**2** showed higher decomposition compared to the other CdS quantum dots due to its higher bandgap. According to the results, the narrower the bandgap the lower the decomposition activity. The size of the nano-catalyst also plays some role since the decomposition efficiency depends on the size of the quantum dots. Since quantum dots are small, the transporting distance of electron-hole from the edges to the surface will as well be limited, as a result it accelerates the movement rate of charge transporters to the surface to partake in the photocatalytic process.

4. Conclusions

We report the preparation, structural, optical and electrochemical studies of ODA-capped CdS quantum dots prepared from thermolysis of three cadmium(II) dithiocarbamate complexes: cadmium(II) phenylpiperazine dithiocarbamate, cadmium(II) imidazolyl dithiocarbamate and cadmium(II) n-hexylaniline dithiocarbamate. The pXRD patterns of the CdS quantum dots were indexed to the zinc blende crystalline phase. The morphological studies of the quantum dots revealed monodispersed spherical particles with crystallite size in the range of 1.92-5.00 nm for ODA-CdS**1**, 2.33-4.66 nm for ODA-CdS**2**, and 3.22-5.21 nm for ODA-CdS**3**. The optical studies of the quantum dots showed absorption band edges are blue shifted. The calculated electrochemical bandgaps are comparable with the optical bandgaps. Photodegradation efficiency of methylene blue dyes was 62% for ODA-CdS**1**, 80% for ODA-CdS**2**, 69% for ODA-CdS**3**. ODA-CdS**2** had high photocatalytic activity and could potentially be applied in the field of dye removal.

References

[1] I. Khan, K. Saeed, I. Khan, Arabian J. Chem., **12**, 908 (2017).

[2] D. A. Yaseen, M. Scholz, Environ. Sci. Pollut. Res. **25**, 1980 (2018).

[3] L. Ngatia, J. M. Grace, D. Moriasi, R. Taylor, Nitrogen and Phosphorus Eutrophication in Marine Ecosystems, in: Monitoring of Marine Pollution, IntechOpen, (2019).

[4] K. Vikrant, B. S. Giri, N. Raza, K. Roy, K.-H. Kim, B. N. Rai, R. S. Singh, Bioresour. Technol. **253**, 355 (2018).

[5] C. Zaharia, D. Suteu, A. Muresan, R. Muresan, A Popescu, Environ. Eng. Manage. J. **8**, 1359 (2009).

[6] M. L. Yola, T. Eren, N. Atar, S. Wang, Chem. Eng. J. **242**, 333 (2014).

[7] R. S. Ashraf, Z. Abid, M. Shahid, Z. U. Rehman, G. Muhammad, M. Altaf, M. A. Raza, Methods for the Treatment of Wastewaters Containing Dyes and Pigments. In: Inamuddin, Ahamed M.I., Lichtfouse E. (eds) Water Pollution and Remediation: Organic Pollutants. Environmental Chemistry for a Sustainable World, vol 54. pp 597-661. Springer, Cham. (2021) https://doi.org/10.1007/978-3-030-52395-4_17

[8] S. Palit, Int. J. Chem. Sci. **10**, 27 (2012).

[9] D. R. Shinde, P. S. Tambade, M. G. Chaskar, K. M. Gadave, Drinking Water Eng. Sci. **10**, 109 (2017).

[10] S. Zhao, P. Song, Z. Wang, H. Zhu, J. Taiwan Inst. Chem. Eng. **82**, 42 (2018).

[11] F. H. Hussein, T. A. Abass, Int. J. Chem. Sc. **8**, 1353 (2010).

[12] S. Dong, J. Feng, M. Fan, Y. Pi, L. Hu, X. Han, M. Liu, J. Sun, J. Sun, RSC Adv. **5**, 14610 (2015).

[13] W.-C. Lin, W.-D. Yang, S.-Y. Jheng, J. Taiwan Inst. Chem. Eng. **43**, 269 (2012).

[14] J. Moma, J. Baloyi, Modified Titanium Dioxide for Photocatalytic Applications, in: Photocatalysts-Applications and Attributes, IntechOpen, 2018.

[15] M. Foszpańczyk, K. Bednarczyk, E. Drozdek, R. Martins, S. Ledakowicz, M. Gmurek, Water Air Soil Pollut. **229**, 362 (2018).

[16] J. Osuwa, C. Oriaku, E. Mgbaja, Chalc. Lett., **7**, 679 (2010).

[17] P. Chawla, G. Sharma, S. Lochab, N. Singh, Bull. Mater. Sci. **33**, 535 (2010).

[18] A. Gadalla, M. A. EL-Sadek, R. Hamood, Chalc. Lett., 15 (2018).

[19] D.C. Hays, B. Gila, S. Pearton, F. Ren, Appl. Phys. Rev. **4**, 021301 (2017).

[20] V. Panchal, D. Errandonea, A. Segura, P. Rodriguez-Hernandez, A. Muñoz, S. Lopez-Moreno, M. Bettinelli, J. Appl. Phys. **110**, 043723 (2011).

[21] A. Shaheen, W. Zia, M.S. Anwar, Band structure and electrical conductivity in semiconductors, LUMS School of Science and Engineering, Lahore, Pakistan, 2011.

[22] A. Sobczyński, A. Dobosz, Polish J. Environ. Stud. **10**, 195 (2001).

[23] C. Jiang, S. J. Moniz, A. Wang, T. Zhang, J. Tang, Chem. Soc. Rev. **46**, 4645 (2017).

[24] A. M. Paca, P. A. Ajibade, Mater. Chem. Phys. **202**, 143 (2017).

[25] P. A. Ajibade, A. A. Fatokun, F. P. Andrew, Inorg. Chim. Acta **504**, 119431 (2020).

[26] I. P. Ferreira, G. M. de Lima, E. B. Paniago, C. B. Pinheiro, J. L. Wardell, S. M. Wardell, Inorg. Chim. Acta. **441**, 137 (2016).

[27] L. L. Mphahlele, P. A. Ajibade, J. Sulfur Chem., **40**, 648 (2019).

[28] P. P. Ingole, Phys. Chem. Chem. Phys. **21**, 4695 (2019).

[29] Y. Jang, A. Shapiro, M. Isarov, A. Rubin-Brusilovski, A. Safran, A. K. Budniak, F. Horani, J. Dehnel, A. Sashchiuk, E. Lifshitz, Chem. Commun. **53**, 1002 (2017).

[30] R. Rajendran, K. Varadharajan, V. Jayaraman, B. Singaram, J. Jeyaram, Appl. Nanosci. **8**, 61 (2018).

[31] D. Ayodhya, M. Venkatesham, A. S. Kumari, G. B. Reddy, D. Ramakrishna, G. Veerabhadram, J. Fluores. **25**, 1481 (2015).

[32] F. P. Andrew, P. A. Ajibade, J. Coord. Chem., 71, 2776 (2018).

[33] F. P. Andrew, P. A. Ajibade, J. Mol. Struct. **1170**, 24 (2018).

[34] J. M. Alyass, A. F. Mohammed, H. Mohammed, Iraqi National J. Chem., 105 (2012).

[35] H. Diarmand-Khalilabad, A. Habibi-Yangjeh, D. Seifzadeh, S. Asadzadeh-Khaneghah, E. Vesali-Kermani, Ceram. Int. **45**, 2542 (2019).

[36] P. A. Kotin, S. S. Bubenov, N. E. Mordvinova, S. G. Dorofeev, Beilstein J. Nanotechnol. **8**, 1156 (2017).

[37] A. Rahdar, V. Arbabi, H. Ghanbari, Int. J. Chem. Biol. Eng. **6**, 81 (2012).

[38] L. Zhang, X. Fu, S. Meng, X. Jiang, J. Wang, S. Chen, J. Mater. Chem. A **3**, 23732 (2015).

[39] N. Ben Brahim, M. L. Poggi, J.-C. Lambry, N. Bel Haj Mohamed, R. Ben Chaâbane, M. Negrerie, Inorg. Chem. **57**, 4979 (2018).

[40] P. A. Ajibade, J. Z. Mbese, B. Omondi, Synth. React. Met.-Org. Inorg. Nano- Met. Chem. **47**, 202 (2017).